

REDESIGN AND MACHINING OF LEADING EDGE OF TRANSONIC COMPRESSOR BLADE IN ROBOTIC GRINDING OPERATION

Heng Li¹, Lai Zou^{1,*}, Wenxi Wang¹ & Lin Gui¹

¹ State Key Laboratory of Mechanical Transmission for Advanced Equipment, Chongqing University, Chongqing, 400044, P.R. China

Abstract

Refined design and machining of the blade, especially the leading edge (LE), are critical for its aerodynamic performance in service. Previous studies have shown a gap in correlation and feedback between design and processing. This study focuses on enhancing performance and size accuracy by redesigning and machining the LE profile of a transonic compressor blade using robotic grinding operations. The LE profile is redesigned based on a clamped B-spline curve to ensure continuous curvature. Then the redesigned and baseline LE shapes in terms of curvature distribution and aerodynamic performance are evaluated. From the robotic grinding perspective, the impact of grinding path numbers on machining efficiency for various LE profiles is analyzed using toolpath planning algorithms. Additionally, the residual errors are predicted using a dwell time control method. A specifically designed airfoil, B3, is selected for a contrast experiment with the baseline, demonstrating higher performance and improved prediction accuracy. Experimental results from robotic grinding show that curvature variation significantly affects machining accuracy and actual performance. The measured mean and RMSE of surface error for B3 are 11.9% and 9.5% lower, respectively, than those of the baseline. However, the sharpness of the ground LE shape is reduced, highlighting the need for a more robust blade shape during optimization to prevent performance losses.

Keywords: Compressor blade; Leading edge; Aerodynamic performance; Robotic grinding

1. Introduction

Efficiency and performance in turbomachinery are critically influenced by the precision of blade design and the accuracy of their manufacturing processes [1, 2]. Among the various components of turbomachinery, the leading edge (LE) of compressor blades plays a pivotal role in determining overall aerodynamic efficiency due to its direct interaction with the airflow at the very forefront of operation [3]. Many studies in the past have been devoted to the optimization of blade shapes, especially LE shapes, to enhance the ideal compressor efficiency [4]. However, the actual blade will inevitably deviate from the design geometry due to the inevitable manufacturing errors, resulting in the aerodynamic performance deviation from the ideal value [5, 6]. Historically, the design and machining of the LE have relied on conventional methods which, while is adequate, often do not fully exploit the potential that modern technology offers.

Recent advances in robotic machining offer significant potential to enhance the precision and variability in blade manufacturing [7, 8]. Particularly, robotic blade grinding can achieve superior surface quality and adherence to aerodynamically optimal profiles compared to traditional methods [9]. However, despite these technological advances, a systematic approach to integrate design improvements with robotic manufacturing processes is often lacking [10]. This integration is crucial, as the aerodynamic performance of blades is highly sensitive to even minute variations in blade geometry, particularly at the LE.

This paper addresses the critical gap in correlating design enhancements with advanced manufacturing techniques. By focusing on the redesign and robotic grinding of the LE profile of a transonic compressor blade, this study aims to establish a more effective methodology that leverages precise robotic grinding capabilities. The redesign utilizes a clamped B-spline curve, optimized for continuous curvature, which is expected to improve the airflow and reduce the aerodynamic drag, thereby enhancing the compressor's efficiency.

2. Redesign and Evaluation of Blade Leading Edge

2.1 Design method based on clamped B-spline curve

The conventional used circular or elliptical LE could cause the discontinuous curvature at the connection point between suction side (SS) and pressure side (PS), which is one of the main reasons for the suction peak of LE. Therefore, in this work, the LE is redesigned based on the Clamped high-order B-spline curve to improve the smoothness of the LE shape and ensure the continuous curvature distribution. The definition of general B spline curve is [11],

$$S(u) = \sum_{i=0}^{n} R_i \cdot N_{i,m}(u), \qquad (1)$$

where R_i is the coordinate of the control point, m is the degree of B-spline curve, $N_{i,m}(u)$ is the basis function, calculated by the recursive formula and the knot vector is $U=[u_0, ..., u_{n+m+1}]$.

$$N_{i,m}(u) = \frac{u - u_i}{u_{i+m} - u_i} N_{i,m-1}(u) + \frac{u_{i+m+1} - u}{u_{i+m+1} - u_{i+1}} N_{i+1,m-1}(u)$$
(2)

There is an additional definition for $N_{i,0}$,

$$N_{i,0} = \begin{cases} 1, u \in [u_i, u_{i+1}) \\ 0, u \notin [u_i, u_{i+1}) \end{cases}$$
(3)

The clamped B-spline curve is a special type of B-spline curve characterized by the fact that by repeating the first and last knot m+1 times [12]. Its two properties are, the first and last control points are exactly the end points of the curve, and the control polygon is tangent to the end points of the curve. Therefore, we can directly determine the coordinates of the first and last control points according to the connection point between the blade profile and the leading edge.

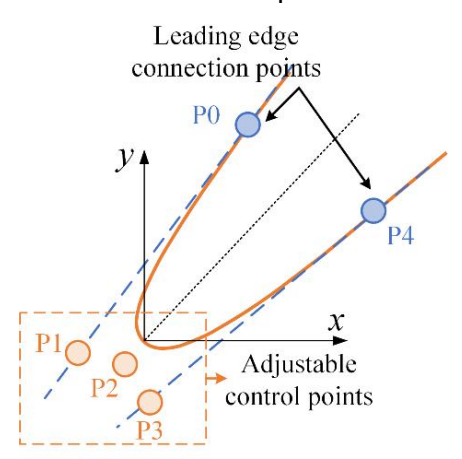


Figure 1 – Principle of LE redesign process.

As shown in Figure 1, P_0 and P_4 are both the LE connection points to the SS and PS, as well as the first and last control points of the LE curve. Another principle to follow is to keep at least C1 continuous at these two junctions. This gives 2 constraint equations,

$$\begin{cases} S'(u_{\min}) = k_0 \\ S'(u_{\max}) = k_1 \end{cases}$$
 (4)

where k_0 and k_1 are the first order derivatives of the SS and PS, respectively, at the connection point. According to the property that the control point polygon of the start end point is tangent to the curve, Eq. (4) is equivalent to that P_1 and P_3 must lie on the tangent line formed by points P_0 and P_4 .

According to the above conditions, the position of P_1 and P_3 on the tangent line can be flexibly adjusted to obtain the four control points. However, in this work, the redesign of the blade shape is based on the constraints of tolerance bands of the baseline. Thus, to freely control the LE shape within the permitted area, it is necessary to additionally introduce the point P_2 , which will increase the flexibility of the design by increasing the curve degree.

The two-dimensional airfoil of 50% span NASA Rotor 37 transonic compressor rotor is selected for redesign. The leading and trailing edges of the baseline are both rounded. To conform to current engineering practice, an elliptical leading edge is constructed as the baseline for subsequent optimization, with the basic geometric parameters [13] given in Table 1. The region of the selected LE profile is 5% (mid-arc) of the arc length range in front of the airfoil.

Table 1 – Baseline airfoil parameters.

Parameter	Value
Chord/mm	56.27
Inlet flow angle/(°)	58.49
Outlet flow angle/(°)	45.86
Mounting angle/(°)	58.38
Grid pitch/mm	38.39
Original LE radius/mm	0.09
LE ellipse axial ratio	1.76

According to the study by xx, the aerodynamic performance can be improved when the geometric deviation of the LE is negative deviation. Therefore, three typical LE profiles within the negative tolerance band are designed by adjusting the coordinates of the control points P_1 - P_3 with the geometric characteristics of close to the SS (B1), mediate between (B2), and close to the PS (B3). The comparison of the three shapes with the baseline is shown in Figure 2.

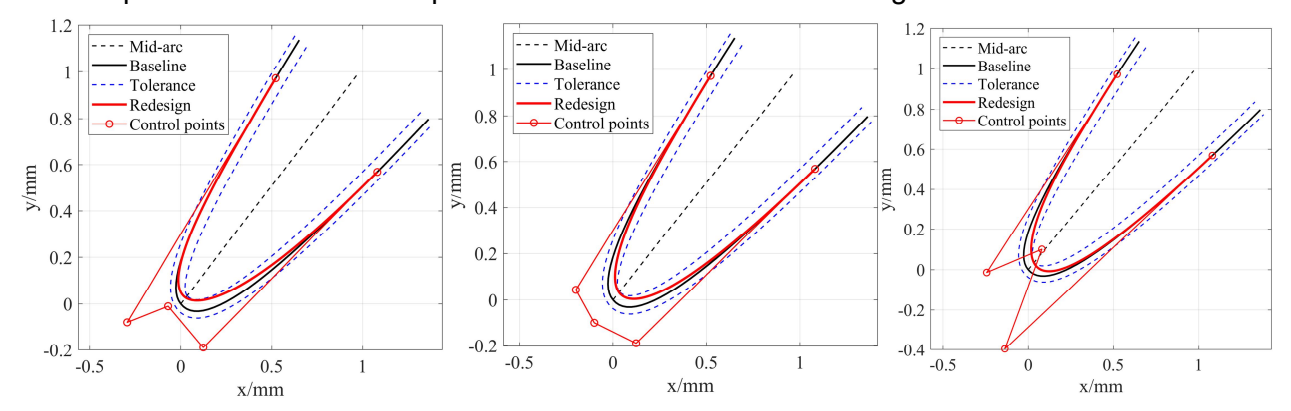


Figure 2 – Designed various LE profiles. (a) B1, close to SS, (b) B2, mediate between, (c) close to PS.

The curvature distributions of the baseline and the three redesigned LE curves are analyzed as shown in Figure 3. The curvature distribution of the original elliptical leading edge shows a discontinuity compared to the redesigned shapes. In contrast, the highest curvature value of B1 is

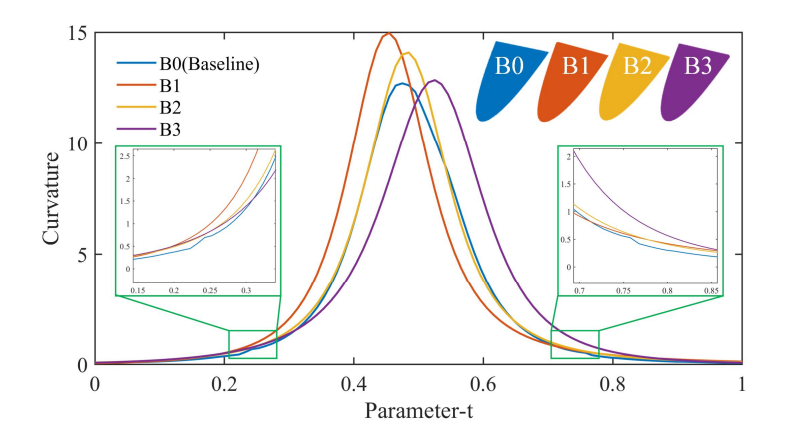


Figure 3 – Comparison of curvature distributions of various LE profiles.

increased by about 13.3% and the location of the highest value is shifted. The curvature of the B2 has also been increased to some extent, with the position of the maximum curvature remaining essentially unchanged. The B3 only show little difference in the highest curvature value but position shifted towards the PS.

The purpose of this work is to redesign and machine the LE in the robotic operation. The redesign process has been completed, and the subsequent evaluation of the redesigned LE profiles will be carried out in two aspects. Firstly, the aerodynamic performance of different LE profiles is evaluated. Secondly, the accuracy and efficiency of the robot grinding process of different LE profiles are provided.

2.2 Aerodynamic performance analysis of various LE profiles

The FINE/Turbo of NUMECA software is used to conduct the two-dimensional numerical calculations for the baseline and redesigned LE profiles. The grid is generated using O4H topology network as shown in Fig. 4.

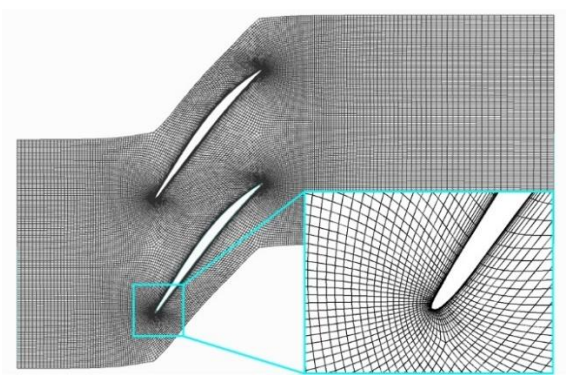


Figure 4 – Computation domain mesh.

The total pressure loss coefficients for various LE profiles are shown in Figure 5. The total pressure loss coefficient is defined as [14],

$$\omega = \frac{\rho_{\text{in}}^{\star} - \rho_{\text{out}}^{\star}}{\rho_{\text{in}}^{\star} - \rho_{\text{in}}},\tag{5}$$

where p^* and p are the total and static pressures, respectively, and in and out represent the inlet and outlet, respectively.

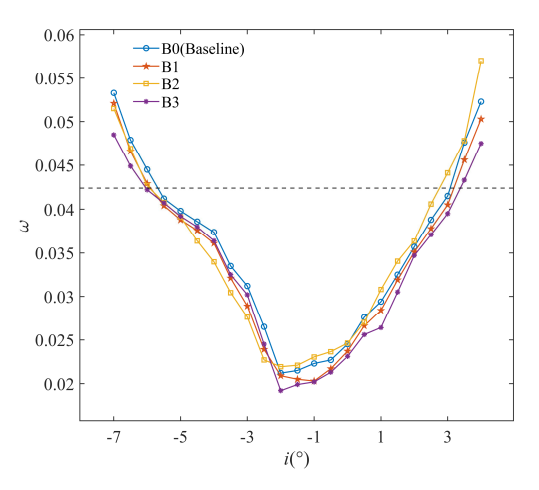


Figure 5 – Variation of total pressure loss coefficient(ω) vs incidence(i) of various LE profiles. The allowable angle of incidence is defined as the angle of attack range corresponding to 1.5 times the lowest total pressure loss coefficient of baseline [15]. As shown by in Figure 6, the allowable angle of incidence for B1 and B3 are increased by 4.09% and 7.96%, respectively, with respect to the baseline airfoil. However, B2 has dropped a little bit, specifically in the positive incidence range. This indicates that the increase in curvature values results in some improvement in performance but

not a linear relationship. Comparing B0 and B3, it is easy to see that the shift of the peak curvature value towards the PS side due to the sharper LE shape can further increase the allowable angle of incidence.

3. Robotic Grinding Method of LE

Different LE profiles imply different surface characteristics, so redesigning the LE profiles shape can also affect robotic grinding operations. This means that enhancement of performance can also lead to the increase in machining difficulty, which is analyzed and discussed in this section specifically in relation to the accuracy and efficiency of robotic grinding process.

3.1 Toolpath planning

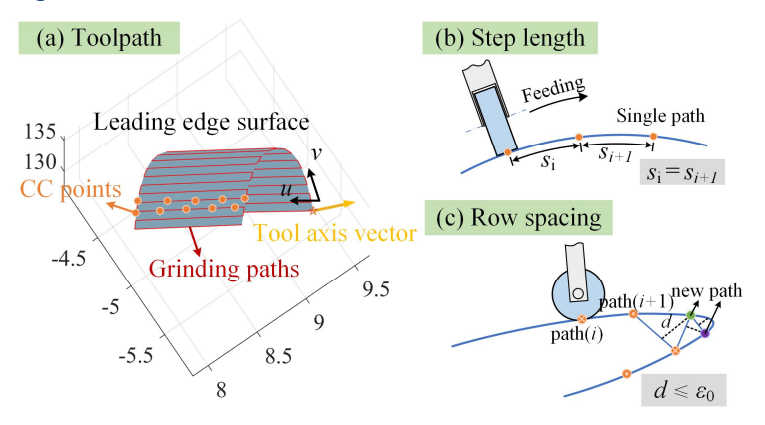


Figure 6 – Toolpath planning method for the leading edge.

The transverse row spacing (v-direction) i.e., longitudinal (u-direction) feeding method is used for grinding. Thus, considering that the curvature variation is small along the u-direction, the equal step method is used to determine the parameter variations between neighboring points ($P_{i,j}$, $P_{i+1,j}$) on the jth grinding path [16]. With a given step size s, the iterative formula for the parameter u is,

$$u(t_{i+1}) \approx u(t_i) + \frac{s}{\sqrt{x'^2 + y'^2 + z'^2}} + \frac{s^2}{2!} \left(-\frac{x'x'' + y'y'' + z'z''}{(x'^2 + y'^2 + z'^2)^2} \right), \tag{6}$$

where $s=S/N_s$ is the step size, S is the total length from the beginning to the end of the parameter u, N_s is the number of machining points set on a single grinding path. (x', y', z') and (x'', y'', z'') are the first-order and second-order derivatives at a point $S(u_i, v_j)$ on the blade surface, respectively.

However, the transverse blade curvature varies dramatically. Thus, the equal step size and chord height error control are combined to determine the row spacing [17]. The initial row spacing is determined in the same way as the step size, and then chord height error between the nearby path is calculated by,

$$d = \left\| \frac{L}{2} - S(\frac{2u_i}{2}, \frac{2v_j + \Delta v}{2}) \right\|$$
 (7)

where $L = \|P_{i,j} - P_{i,j+1}\|$ is the distance between two neighboring grinding path for fixed u_i . If $d < \varepsilon_0$ is satisfied, no correction is required. Otherwise, the point on the curve corresponding to the middle node of these two points is taken as a new point and stored i.e., $\Delta v = \Delta v/2$ and the new parameter $v_{j+1} = v_j + \Delta v$ is updated for $P_{i,j+1}$. The determination of chord height error continues until all adjacent

points meet the requirements.

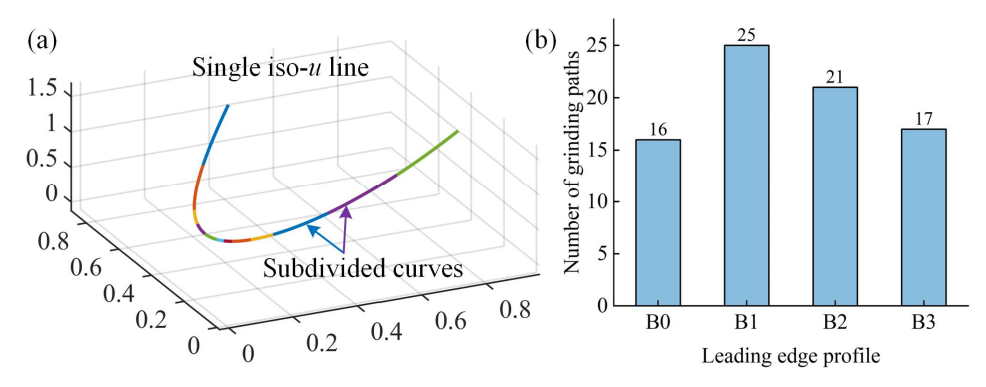


Figure 7 – Toolpath planning results of various LE profiles. (a) Row spacing, (b) Number of grinding paths.

Compared to the baseline, the aerodynamic performance of the three redesigned LE profiles are improved, but this is offset by a decrease in grinding efficiency in terms of grinding paths. Figure 3 shows that the curvature of B1-B3 increased compared to B0, with B3 showing the smallest change. Therefore, with the same chord height threshold constraint, the number of planned paths obtained for B3 is also only one more than for B0. If the subsequent grinding accuracy can be guaranteed, then this slight loss in efficiency of B3 is acceptable in exchange for the performance improvement. Having obtained the CC points by discretizing the LE surface, the next step is to regulate the grinding parameters, which has the greatest impact on the machining accuracy.

3.2 Grinding parameter regulation

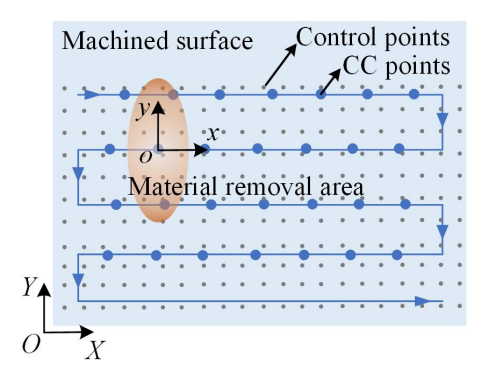


Figure 8 – Diagram of grinding effect of each CC points on control points.

The process on the LE surface along the grinding path can be simplified as shown in Figure 8. During machining, the grinding tool passes through each CC point with given grinding parameters. The target is to remove excess material from the entire machined surface to achieve the desired surface finish. Therefore, dense sampling points are introduced on the machined surface. When planning grinding parameters such as grinding speed, feed rate and grinding pressure, it is only necessary to ensure that the residual material corresponding to these sampling points is removed [18].

Firstly, there is a unique grinding removal profile of each CC point due to the various curvature as well as the grinding time. To determine the range of influence of the removal function for each CC point, traversing its removal depth for all sampling points is necessary to get a removal vector \mathbf{h}_i .

$$\boldsymbol{H} = \begin{bmatrix} h_{1,1} & h_{1,2} & \cdots & h_{1,n} \\ h_{2,1} & h_{2,2} & \cdots & h_{2,n} \\ \vdots & \vdots & \ddots & \vdots \\ h_{m,1} & h_{m,2} & \cdots & h_{m,n} \end{bmatrix}, \boldsymbol{h} = \begin{bmatrix} h_{i,1} \\ h_{i,2} \\ \vdots \\ h_{i,m} \end{bmatrix}$$
(8)

Knowing the curvature information of the tool contact point solving for the removal profile of a flexible abrasive at that point is a complex problem. Our previous work [19] developed a model to establish the relationship between grinding parameters, curvature information, abrasive tool properties and removal depth h as Eq.9.

$$h(x,y) = \int_0^t Nk(\frac{9p(x,y)^2 R_g \pi^2}{16F^{*4/3}} - d_0) v_s dt$$
 (9)

Next, the traversal results of all CC points are integrated to obtain the global material removal matrix H. Based on the sampling point mesh, the allowance distribution can be extracted by comparing the theoretical model and the unprocessed surface. Based on these three steps, the solution equation for the dwell time can be obtained as Eq.8. Theoretically, if the dwell time vector t can satisfy this equation, the unprocessed allowance can be removed.

$$Ht = R, t = \begin{bmatrix} t_1 \\ t_2 \\ \vdots \\ t_n \end{bmatrix}, R = \begin{bmatrix} r_1 \\ r_2 \\ \vdots \\ r_m \end{bmatrix}$$
(10)

However, the number of sampling points *m* tends to be much larger than the number of CC points *n*, results in Eq. 8 being a super-determined system of non-linear equations with no exact solution. For such problems, the least squares method with boundaries is an effective solving technique. Additionally, Tikhonov regularization needs to be introduced to address ill-conditioned problems as shown below [20],

min
$$\frac{1}{2} \| \mathbf{H} \mathbf{t} - \mathbf{R} \|_{2}^{2} + \frac{1}{2} \beta \| \mathbf{t} \|_{2}^{2}$$
 $(\beta > 0)$
s.t. $\mathbf{t} > 0$ (11)

where β is the Tikhonov regularization factor.

Surface error could be defined according to the calculation results,

$$rs = R - Ht$$
 (12)

3.3 Prediction and evaluation of designed LE shapes

Based on Eq. 12, the prediction of surface error for unprocessed blades can be carried out. The LE of the blade has a significant impact on aerodynamic performance and is also difficult to achieve precisely grinding. Therefore, the limitation of machining capability must be considered when carrying out the optimization design of LE shape. It is necessary to evaluate the machinability of the four airfoils designed in Section 1 in robotic grinding operations.

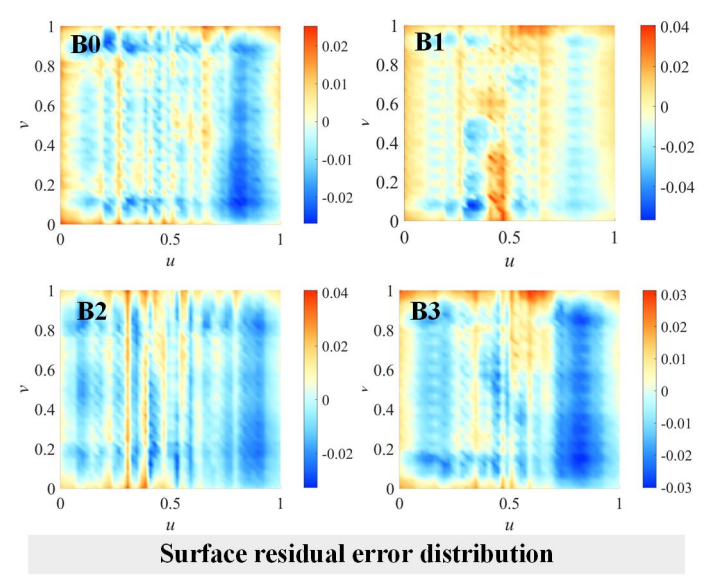


Figure 9 – Comparison of the predicted surface residual error of various blade.

As displayed in Figure 9, the predicted surface error for the three redesigned airfoils increases to some extent compared to the baseline (B0). For B1, although the allowable angle of incidence range is increased, this is at the expense of reduced machining accuracy. The 3D residual error has nearly doubled. The aerodynamic performance of B2 show no improvement, but the predicted machining accuracy is reduced due to the faster curvature change. As discussed in Section 1, the aerodynamic

performance of B3 is also improved. The upper and lower limits of its predicted residual error is ± 0.03 mm, which can meet the common blade machining requirements. If machining errors can be controlled within acceptable value, the B3 LE blade shape can be considered a more desirable optimized result for current robotic grinding operations by guaranteeing performance and machinability.

According to the curvature distribution and predicted residual error of these four airfoils, the sharpness of the LE shape is one of the key factors affecting its machining accuracy. Therefore, B3 and baseline are selected for verification in the next section of the grinding experiment. If the ground LE shape can still be maintained after actual machining, the performance of the actual blade can be improved.

4. Grinding Experiments

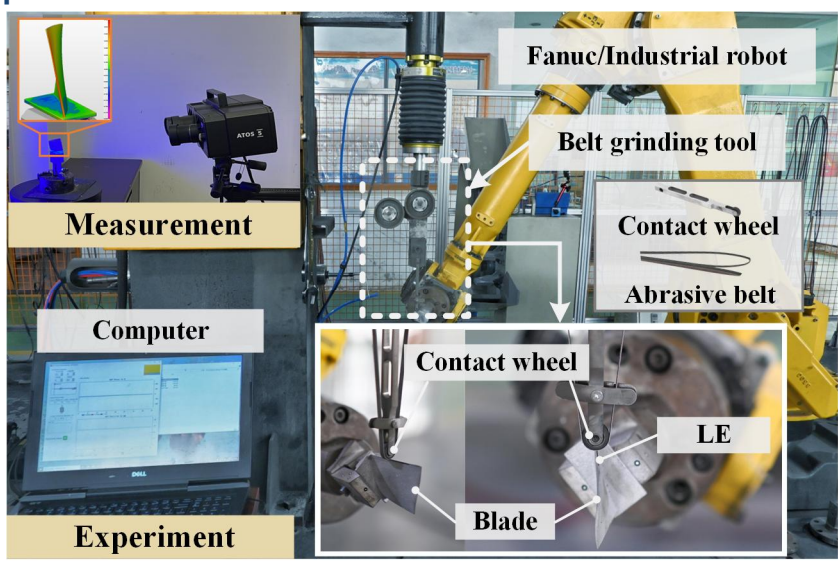


Figure 10 – Diagram of grinding effect of each CC points on control points.

The experiment platform for robotic belt grinding is shown in Fig.10. Pre- and post-grinding measurements of the blade profile are conducted using the ATOS-5 optical scanner from GOM, offering a measuring precision up to 0.005mm within a single frame measurement range of 100mm by 70mm. A 6-axis FANUC industrial robot is M-710iC-50 is used. Throughout the grinding procedure, a consistent normal contact force of 5 N is maintained, controlled by a pneumatic constant force mechanism (ACF-111/04, FERROBTICS). The grinding tool is consisting of the drive wheels, a rubber contact wheel and abrasive belt, which is linked with the constant force unit. More detailed grinding parameters are listed in Tab.2.

Table 2 – Robotic	grinding	experimental	parameters.

Parameters	Value
Grinding speed	6 m/s
Feed rate	Point-by-point regulation
Normal contact force	5 N
Abrasive belt	Pyramidal abrasive belt
Grain size	A6/P2000
Contact wheel	Ф15 mm×5 mm with 50HA
Blade material	AlSi10Mg

5. Results and Discussions

Figure 11 demonstrates the comparison of the experiment results of baseline and B3. It can be found that the residual error distribution is different from the predicted due to the inevitable error of grinding system and material removal model. Fortunately, the residual error value was well controlled. The conventional required tolerance band for compressor blades is -0.05mm~+0.05mm, which is large than the error distribution.

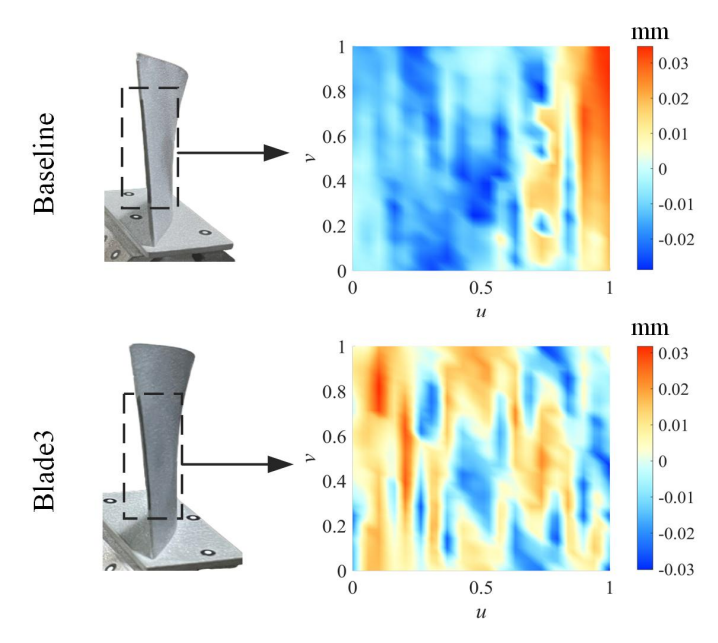


Figure 11 – Ground blade LE and residual error distribution.

Further analysis shows that the consistency of the deviation distribution of Blade 3 is better than that of the baseline. The mean absolute values of the deviations of baseline and B3 are 0.0134mm and 0.0119mm, respectively, and the RMSE value are 0.0157mm and 0.0142mm, respectively. Compared to the baseline, these two indicators of B3 were reduced by 11.9% and 9.5%, respectively. In addition to the distribution of errors across the entire machined surface, the fidelity of the two-dimensional cross-sectional shape is also an important indicator of grinding quality. Therefore, a comparative analysis of the cross-sectional line shapes of the two types of blade machining was conducted, as shown in Figure 12.

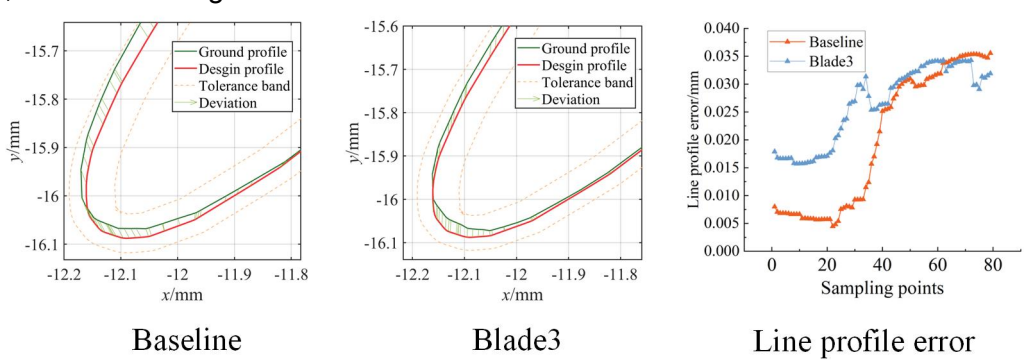


Figure 12 – Cross-section of ground LE and line profile error.

The figure shows that the reason for the significant fluctuation in surface error of baseline is due to a slight shift of the actual LE profile towards the PS, causing significant positive and negative deviations. For the B3, although the absolute deviation is smaller, the sharpness of the LE after machining decreases significantly, which results in a loss of aerodynamic performance. Therefore, when aiming to enhance aerodynamic performance through LE shape optimization, merely considering theoretical model improvements is insufficient. It is more important to design blade shapes with high robustness to manufacturing errors of the final processing operation.

6. Conclusion

In this work, redesign and machining of the LE were carried out for enhancing the aerodynamic performance and size accuracy of a transonic compressor blade in robotic grinding operations. The LE profile was redesigned based on a clamped B-spline curve to ensure continuous curvature. Evaluations of the redesigned and baseline LE shapes were conducted in terms of curvature distribution and aerodynamic performance. From the perspective of robotic grinding, the machining efficiency and predicted residual errors across various LE profiles showed B3 is a more desire LE shape. Thus, it was chosen for a contrast experiment with the baseline. The results indicated that

variations in curvature significantly influence machining accuracy and actual performance. The measured mean and RMSE of surface error for B3 were found to be 11.9% and 9.5% lower, respectively, than those of the baseline. However, a reduction in the sharpness of the ground LE shape was observed. The findings underscore the potential improvements in blade aerodynamic performance and machining precision through LE profile optimization. However, the decrease in sharpness post-machining poses a negative impact on performance. Future work should therefore focus on maintaining blade sharpness through advanced machining techniques and optimized design parameters.

7. Contact Author Email Address

The contact author email is: zoulai@cqu.edu.cn

8. Acknowledgement

This study was supported by the National Natural Science Foundation of China (52075059), Graduate Scientific Research and Innovation Foundation of Chongqing (CYB23021) and National Natural Science Foundation of Chongqing (CSTB2024NSCQ-MSX0784).

9. Copyright Statement

The authors confirm that they hold copyright on all of the original material included in this paper. The authors also confirm that they have obtained permission, from the copyright holder of any third party material included in this paper, to publish it as part of their paper. The authors confirm that they give permission, or have obtained permission from the copyright holder of this paper, for the publication and distribution of this paper as part of the ICAS proceedings or as individual off-prints from the proceedings.

References

- [1] Li Z, Zheng X. Review of design optimization methods for turbomachinery aerodynamics. *Progress in Aerospace Science*. Vol. 93, pp 1-23, 2017.
- [2] Lin J, Zhang J, Zhang G, Ni G, Bi F. Aero-engine blade fatigue analysis based on nonlinear continuum damage model using neural networks. *Chinese Journal of Mechanical Engineering*. Vol. 2, pp 338-345, 2012.
- [3] Ma C, Gao L, Wang H, Li R, Wu B. Influence of leading edge with real manufacturing error on aerodynamic performance of high subsonic compressor cascades. *Chinese Journal of Aeronautics*. Vol. 34, pp 220-232, 2021.
- [4] Song Z, Zheng X, Wang B, Zhou K, Amankwa A.R. Multidisciplinary robust optimization approach of fan rotors under structural constraints with blade curvature. *Aerospace Science and Technology*. Vol. 142 pp 108637, 2023.
- [5] Wang X, Zou Z. Uncertainty analysis of impact of geometric variations on turbine blade performance, *Energy.* Vol. 176, pp 67-80, 2019.
- [6] Liu Y, Ju Y, Qin R, Jiang W, Spence S, Zhang C. Collaborative Robust Design Optimization of Blade Geometry and Manufacturing Tolerance for a Transonic Centrifugal Impeller. *Journal of Turbomachinery*. Vol. 145, pp 071001, 2023.
- [7] Wang Q, Wang W, Zheng L, Yun C. Force control-based vibration suppression in robotic grinding of large thin-wall shells. *Robotics and Computer-Integrated Manufacturing*. Vol. 67, pp 102031, 2021.
- [8] Ge J, Deng Z, Li Z, Liu T, Zhuo R, Chen X. Adaptive parameter optimization approach for robotic grinding of weld seam based on laser vision sensor. *Robotics and Computer-Integrated Manufacturing*. Vol. 82, pp 102540, 2023.
- [9] Zhu D, Xu X, Yang Z, Zhuang K, Yan S, Ding H. Analysis and assessment of robotic belt grinding mechanisms by force modeling and force control experiments. *Tribology International*. Vol. 120, pp 93-98, 2018.
- [10]D. Zhu, X. Feng, X. Xu, Z. Yang, W. Li, S. Yan, H. Ding. Robotic grinding of complex components: A step towards efficient and intelligent machining challenges, solutions, and applications. *Robotics and Computer-Integrated Manufacturing*. Vol. 65, pp 101908, 2020.
- [11]Li Z.L, Wang R, Zhang X.Q. B-spline surface approximation method for achieving optimum dwell time in deterministic polishing. *Journal of Materials Processing Technology.* Vol. 318, pp 118031, 2023.
- [12] Chen C, Khan M.A. Piecewise b-spline tool paths with the arc-length parameter and their application on high feed, accurate CNC milling of free-form profiles. *Journal of Manufacturing Science and Engineering*. Vol. 134, pp 1-13, 2012.
- [13]M. Mohsen, F.M. Owis, A.A. Hashim, The impact of tandem rotor blades on the performance of transonic

- axial compressors, Aerospace Science and Technology. Vol. 67, pp 237-248, 2017.
- [14]Ju Y, Liu Y, Jiang W, Zhang C. Aerodynamic analysis and design optimization of a centrifugal compressor impeller considering realistic manufacturing uncertainties, *Aerospace Science and Technology*. Vol. 115, pp 106787, 2021.
- [15]Goodhand M.N, Miller R.J, Lung H.W. The impact of geometric variation on compressor two-dimensional incidence range. *Journal of Turbomachinery*. Vol. 137, No. 2, pp 1-7,2015.
- [16]Lv C, Zou L, Huang Y, Liu X, Li Z, Gong M, Li H. A trajectory planning method on error compensation of residual height for aero-engine blades of robotic belt grinding, *Chinese Journal of Aeronautics*. Vol. 35, pp 508-520, 2022.
- [17]Lv C, Zou L, Huang Y, Li H, Wang T, Mu Y. A Novel Toolpath for Robotic Adaptive Grinding of Extremely Thin Blade Edge Based on Dwell Time Model. *IEEE/ASME Transactions on Mechatronics*. Vol. 27, pp 4429-4439, 2022.
- [18]Dong Z, Cheng H. Toward the complete practicability for the linear-equation dwell time model in subaperture polishing. *Applied Optics*. Vol. 54, pp 8884-8890, 2015.
- [19]Li H, Zou L, Lv C. Collaborative improvement of profile accuracy and aerodynamic performance in robotic grinding of transonic compressor blade leading edge. *Aerospace Science and Technology*. Vol. 146, pp 108937, 2024.
- [20]Peng Y, Shen B, Wang Z. Review on polishing technology of small-scale aspheric optics. *The International Journal of Advanced Manufacturing Technology*. Vol. 115, No. 4, pp 965-987, 2021.